International Journal of Nanomedicine

Dovepress
Taylor & Francis Group

Open Access Full Text Article

ORIGINAL RESEARCH

Neutrophil-Membrane Biomimetic Hollow Mesoporous Silica Nanoparticles for Targeted Delivery of Imperatorin to Alleviate Cerebral Ischemia–Reperfusion Injury via Nrf2/ARE/Keap1 Pathway

Feifei Chen[1,*], Hui Jiang[2,*], Xueyi Song[3], Jianfeng Wang[3], Xu Ma[4], Quan Zhou[3], Abdullah Al Mamun[5], Lingna Li[6], Yunfang Zhou[3], Hongbin Xu[1], Shuanghu Wang[3]

[1]Department of Pharmacy, The First Affiliated Hospital of Ningbo University, Ningbo, 315010, People's Republic of China; [2]Department of Pharmacy, The People's Hospital of Guangxi Zhuang Autonomous Region, Guangxi Academy of Medical Sciences, Nanning, 530021, People's Republic of China; [3]Central Laboratory of Lishui Hospital of Wenzhou Medical University, The First Affiliated Hospital of Lishui University, Lishui People's Hospital, Lishui, 323000, People's Republic of China; [4]Department of Pediatric Orthopaedics, Maternal and Child Health Hospital of Guangxi Zhuang Autonomous Region, Nanning, 530003, People's Republic of China; [5]Department of Pharmacy, American International University-Bangladesh (AIUB), Dhaka, 1229, Bangladesh; [6]Department of Pharmacy, The Affiliated Hospital of Ningbo University, LiHuiLi Hospital, Ningbo, 315010, People's Republic of China

*These authors contributed equally to this work

Correspondence: Hongbin Xu; Shuanghu Wang, Email xuhongbin@tongji.edu.cn; wangshuanghu@lsu.edu.cn

Introduction: Cerebral ischemic stroke has high mortality and disability rates with limited targeted therapeutic strategies. Biomimetic nanocarriers can optimize drug delivery efficiency and exert neuroprotection effects, providing a promising strategy for ischemia-reperfusion injury treatment.

Methods: Hollow mesoporous silica nanoparticles (HMSNs) were synthesized via an improved Stoer method and loaded with imperatorin (IMP). Subsequently, neutrophil cell membranes (NCM) extracted from DMSO-induced HL-60 cells were coated onto the nanoparticles to construct NCM/IMP@HMSNs. Nanomaterial characterization was carried out. In vitro oxygen-glucose deprivation/reoxygenation (OGD/R) models in SH-SY5Y cells and in vivo rat middle cerebral artery occlusion/reperfusion (MCAO/R) models were established to explore the underlying neuroprotective mechanisms.

Results: The synthesized NCM/IMP@HMSNs nanoparticles possessed uniform particle size (~143 nm) and favorable stability, with an encapsulation efficiency of 31.84%. In vitro results revealed that IMP significantly increased the viability of OGD/R-injured SH-SY5Y cells compared with the model group. In vivo experiments showed that NCM/IMP@HMSNs efficiently accumulated in ischemic brain tissue, notably decreased mNSS scores, and reduced cerebral infarct volume by approximately 33.31% compared with the MCAO/R group. This nanosystem activated the Nrf2/ARE/Keap1 pathway, thereby upregulating HO-1 expression to strengthen antioxidant capacity, alleviate the accumulation of cerebral oxidative stress products, and regulate the activities of SOD, GSH, CAT and LDH.

Conclusion: The biomimetic NCM/IMP@HMSNs nanoplatform enhances the neuroprotective efficacy against ischemia–reperfusion injury via activating the Nrf2/ARE/Keap1 pathway, offering a promising targeted therapeutic approach for ischemic stroke therapy.

Keywords: ischemic stroke, hollow mesoporous silica nanoparticles, imperatorin, Nrf2/ARE/Keap1 pathway

Introduction

Stroke, also known as "cerebral stroke" or cerebrovascular accident, is most common among middle-aged and elderly people. Clinically, 80% of strokes are associated with cerebral ischemia, mainly caused by cerebrovascular thrombosis or embolism.[1,2] The goal of clinical treatment for ischemic stroke is to restore blood perfusion to the ischemic foci as

https://doi.org/10.2147/IJN.S592970
Received: 27 January 2026
Accepted: 3 June 2026
Published: 8 June 2026

quickly as possible in order to "salvage" brain function.[3] After reperfusion in ischemic stroke, neurons in the ischemic brain region regain oxygenation, oxidative stress rapidly occurs, and inflammatory cells accumulate in and around the lesion, further exacerbating brain tissue damage.[4,5] Thus, there is an urgent need to develop effective therapeutic strategies for alleviating ischemic reperfusion injury.

Traditional Chinese Medicine (TCM) has a wealth of experience in preventing and treating diseases.[6] Imperatorin (IMP) belongs to the group of 6, 7-furanocoumarins, which are widely distributed in natural medicinal plants such as *Angelica dahurica, Saposhnikovia divaricata* and *cnidium monnieri*. It has a wide range of pharmacological effects: analgesic, anti-inflammatory, anti-tumor, anti-bacterial, anti-hypertensive, anti-viral, anti-apoptotic and neuroprotective.[7,8] IMP is a promising treatment for oxidative stress and an inhibitor of inflammatory responses in cerebral ischemia-reperfusion.[9] However, IMP exhibits poor metabolic stability in the gastrointestinal tract and low oral bioavailability, limiting its therapeutic potential.[10] In addition, drugs used in brain diseases are often difficult to cross the blood-brain barrier, and cannot be enriched at the disease site to achieve effective therapeutic concentration, which limits their clinical use.

In recent years, nanomedicine and nanoparticles delivery systems have developed rapidly, with great advances in the field of biology. Meanwhile, nanomedicines have gained widespread attention in the world. Small-sized nanoparticles can cross certain physiological barriers, and targeted drug delivery systems enable precise drug delivery.[11,12] They exhibit typical endocytosis mechanisms in vivo, resulting in high oral bioavailability, and the nanocarriers can remain in the circulatory system for a long period of time and are capable of releasing a mixture of drugs in a specified dosage. Cellular uptake of nanostructures is much higher than that of large particles with diameters between 1 and 10 μm, and polymeric nanomaterials with diameters between 10 and 1000 nm are ideal carriers for efficient delivery.[13] Nanoparticles as drug delivery platforms can be used to deliver drugs more precisely to target tissues by surface binding or loading them with controlled and sustained release.[14,15] Hollow mesoporous silica nanoparticles (HMSNs) are inorganic polymeric nanomaterials with a customizable mesoporous structure, a high specific surface area and pore volume, and good biosafety.[16,17] These properties confer unique advantages to HMSNs, which have led to the development of effective drug delivery systems for a wide range of therapeutic agents.

Modification on the surface of nanoparticles can change their surface properties, thereby altering the physicochemical properties of nanomaterials such as biological half-life, biocompatibility, bioavailability, and metabolic stability. The use of cell membrane encapsulation to make nanoparticles biomimetic and biologically safe not only prolongs the circulation time of nanocarriers by avoiding immune clearance, but also imparts some intrinsic cellular properties to the nanoparticles, such as specific targeting of inflammatory regions, selective adherence, immune evasion, endothelial penetration, and increased affinity for binding to targeted receptors.[18] Biomimetic neutrophil membrane nanosystems have achieved promising therapeutic effects in cerebral ischemia-reperfusion models by inhibiting inflammation and neuronal apoptosis.[19] In terms of membrane sources, primary neutrophils have short lifespan and need to be used within 2–4 hours after isolation.[20] Donor individual differences also lead to poor batch stability. In contrast, HL-60 cells are a feasible alternative, which can be stably expanded and cryopreserved in large quantities to guarantee stable yield and good repeatability.[21] Nevertheless, we admit that HL-60 cell-derived membranes differ from primary neutrophil membranes in surface protein composition and biological functions. Currently, mainstream nanotherapies for ischemic stroke, such as liposomes, polymeric and inorganic nanoparticles, are restricted by low lesion enrichment efficiency, immune clearance and residual neurotoxicity, limiting clinical translation.[22,23] In contrast, neutrophil membrane-biomimetic nanocarriers possess unique inflammatory tropism toward damaged cerebral blood vessels, reducing non-specific accumulation and long-term neurotoxic risks in brain parenchyma, and thereby improving biosafety.[24,25] Despite limitations in membrane storage stability, scalable production and long-term in vivo metabolism, it still has certain advantages for ischemic stroke treatment.

Inspired by above, we attempted to form a biomimetic drug delivery system for the treatment of ischemic stroke (Scheme 1). The platform consists of HMSNs loaded with IMP as the core and the outer layer wrapped around the neutrophil-like membrane, which ultimately forms the biomimetic NCM/IMP@HMSNs delivery system. We extracted the nanovesicles from DMSO-induced human leukemia cells, HL-60 cells, which functionally resemble the surface of neutrophil membranes, and used HMSNs loaded with antioxidants to enhance the stability of the antioxidants by

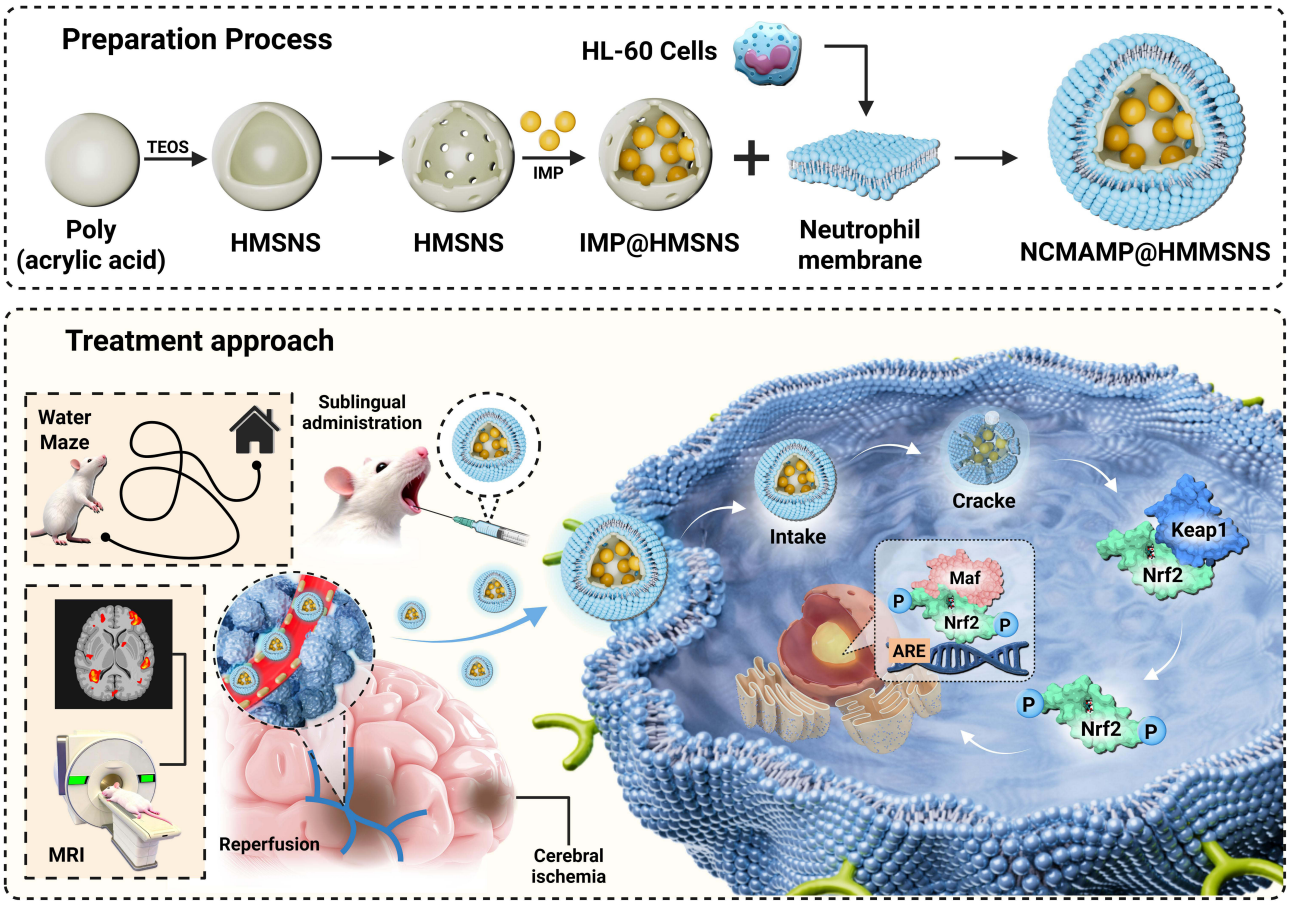

Scheme 1 Schematic of biomimetic NCM/IMP@HMSNs drug delivery system for targeted therapy in cerebral ischemia-reperfusion injury via oxidative stress modulation.

providing them with a protective shell preventing their decomposition and prolonging the blood half-life. In this study, HMSNs were prepared by a modified Stoer method using polyacrylic acid (PAA) as a template and Tetraethyl orthosilicate (TEOS) as a silica source, and HMSNs nanoparticles with a hollow mesoporous structure were prepared. Our results indicate that NCM/IMP@HMSNs nanoparticles hold promise as a promising therapeutic approach for ischemic stroke reperfusion injury.

Materials and Methods

Materials

PAA was purchased from Acros Organics, Germany. PEG-200 was obtained from Shanghai Aladdin Biochemical Technology Co., Ltd. All cell culture reagents were purchased from Gibco (Thermo Fisher Scientific). BCA assay kit was obtained from Solarbio Science & Technology Co., Ltd., Beijing. Antibodies against CD11b, CD18, Calnexin, Nrf2, Keap1 and HO-1 were supplied by Proteintech Group, Inc, while β-actin antibody was purchased from Cell Signaling Technology, USA. LDH, GSH, SOD, MDA and CAT assay kits were all acquired from Nanjing Jiancheng Bioengineering Institute.

Preparation of the IMP@HMSNs Delivery System

HMSNs were prepared via the modified Stoer method.[26] First, 153.8 μL of PAA (50 wt%) was fully dissolved in 1.5 mL of aqueous ammonia (25–28 wt%) to obtain an ammonia solution of the polyelectrolyte. This solution was added to 30 mL of absolute ethanol under stirring, and a large number of colloidal aggregates formed. Subsequently, 750 μL of TEOS was added in portions within 10 hours. After the final addition, the mixture was stirred for 2 hours and then

https://doi.org/10.2147/IJN.S592970

allowed to stand for aging for 4 hours to ensure uniform silica deposition. HMSNs were collected by centrifugation, and the precipitate was dispersed in absolute ethanol for storage. Seventy milligrams of HMSNs were uniformly dispersed in 20 mL of absolute ethanol solution of IMP (5 mg/mL). The mixture was stirred for 48 hours at room temperature under protection from light. The precipitate was collected, uniformly dispersed in water, and stored for subsequent use. The drug loading behavior was analyzed by determining the IMP content in the supernatant after drug loading using UPLC-MS/MS. The encapsulation efficiency and drug loading capacity of IMP were calculated using the following formulas, respectively. All measurements were performed in triplicate, and the average value was taken.

Encapsulation efficiency (EE%) = (Amount of drug loaded in HMSNs/Total initial drug amount) × 100% (1)

Drug loading capacity (LC%) = (Amount of drug loaded in HMSNs/Total weight of drug-loaded HMSNs) × 100% (2)

Characterization of Nanoparticles

The particle size and zeta potential of HMSNs were determined using a Malvern Zetasizer Nano ZS 90 laser nanoparticle size analyzer. The morphology of HMSNs nanoparticles was observed via Transmission Electron Microscopy (TEM) and Scanning Electron Microscopy (SEM).

In vitro Drug Release Evaluation

The in vitro release behavior of IMP@HMSNs was investigated via the dialysis method at 37°C. First, the IMP@HMSNs were fully dispersed and then into dialysis bags with a molecular weight cutoff of 8000 Da, which were subsequently immersed in 0.5% Tween 80 solutions with pH7.4 and pH6.8. At predetermined time intervals (20min, 40min, 1h, 2h, 3h, 4h, 6h, 8h, 12h, 24h, 48h and 72h), 1 mL of the release medium was withdrawn, and an equal volume of fresh solution was immediately added to maintain a constant total volume. The cumulative release amount of IMP was determined by UPLC-MS/MS.

Extraction of HL60 Cell Membranes

The extraction of HL60 cell membranes was performed according to the manufacturer's instructions. First, HL60 cells induced for 4–6 days were collected and added to Membrane Protein Reagent A pre-mixed with PMSF at a density of 5×10^7 cells/mL. The cells were gently resuspended and incubated on ice for 15 minutes. The cell suspension was subjected to cell disruption using a cryogenic grinder, and the disruption efficiency was confirmed by microscopic observation. The supernatant was collected by centrifugation and transferred to a new EP tube. The precipitate was then collected by centrifugation at 14,000 × g and stored for subsequent use.

Detection of Neutrophil Membrane Characteristics Expressed on HL-60 Cell Membranes

Protein extraction was performed on undifferentiated HL-60 cell membranes (NHM) and differentiated HL-60 cell membranes (NCM). The expression levels of neutrophil surface markers CD11b, CD18 and calnexin on the cell membranes were detected by Western Blot assay.

Preparation of the NCM/IMP@HMSNs Delivery System

The differentiated cell membranes were uniformly dispersed in an appropriate amount of normal saline and loaded into a liposome extruder. The mixture was sequentially extruded through 1 μm and 400 nm polycarbonate membranes to form cell membrane vesicles. Finally, the vesicles were mixed with IMP@HMSNs at a volume ratio of 1:1, and the mixture was extruded through a 200 nm porous polycarbonate membrane to obtain membrane-wrapped NCM/IMP@HMSNs.

Cell Culture

The human neuroblastoma cell line SH-SY5Y was purchased from Wuhan Procell Life Science & Technology Co., Ltd. SH-SY5Y cells were cultured in RPMI-1640 medium supplemented with 10% fetal bovine serum (FBS) and 1% penicillin/streptomycin (P/S) mixture, and maintained in a cell incubator at 37°C with 5% CO_2.

Drug Uptake of HMSNs in SH-SY5Y Cells

SH-SY5Y cells in the logarithmic growth phase were seeded into 12-well plates with coverslips attached to the bottom at a density of approximately 5×10^4 cells/well. After the cells adhered overnight, they were starved for 6 hours using serum-free RPMI-1640 medium. Subsequently, the cells were cultured routinely for 24 hours in complete medium containing rhodamine B-loaded HMSNs and PKH67-fluorescently labeled NCM/IMP@HMSNs, respectively. After 24 hours, the medium was aspirated, and the cells were washed with PBS. The cells were then fixed with 4% paraformaldehyde solution. The coverslips were removed from the 12-well plates, inverted and placed on glass slides drop-coated with DAPI-containing anti-fade mounting medium, and observed immediately under a fluorescence microscope.

Establishment of the Oxygen-Glucose Deprivation/Reperfusion (OGD/R) Model in SH-SY5Y Cells

SH-SY5Y cells were seeded into 96-well plates at a density of 1×10^5 cells/mL and allowed to adhere overnight. When the cells grew to 60%, the original complete medium of the cells in the model group was aspirated. After washing with PBS, the medium was replaced with serum-free and low-glucose DMEM medium. The cells were cultured in a tri-gas incubator (37°C, 1% O_2, 5% CO_2, and 94% N_2) for 1, 2, 3, 6, 9, and 12 hours to induce oxygen-glucose deprivation (OGD). After the low-glucose and hypoxic culture, the serum-free low-glucose DMEM medium was replaced with complete medium, and the cells were routinely cultured in a 37°C, 5% CO_2 cell incubator for 24 hours to achieve glucose and oxygen reperfusion (R). At the end of the routine culture, the 96-well plate was taken out, gently washed three times with PBS, and fresh complete medium was added to avoid the interference of dead and floating cells caused by model establishment on the subsequent absorbance measurement. Ten microliters of CCK-8 reagent was added to each well, followed by thorough mixing by shaking. The plate was returned to the incubator for another 1 hour of culture. The absorbance value was measured at 450 nm using a microplate reader to calculate cell viability. The OGD/R model establishment protocol was selected based on a cell viability of 50%–60%.

Western Blot

SH-SY5Y cells were seeded into 6-well plates and incubated overnight at 37°C. After 24 hours of incubation, the cells were washed twice with PBS, followed by the addition of RIPA lysis buffer and incubation for 10 minutes. The mixture was centrifuged at 12,000 rpm at 4°C, and the supernatant was collected. The protein concentration was determined using a BCA protein assay kit. After separation by 10% sodium dodecyl sulfate-polyacrylamide gel electrophoresis (SDS-PAGE), the proteins were electrotransferred onto polyvinylidene fluoride (PVDF) membranes. The membranes were blocked with 5% non-fat milk for 1 hour, then incubated with primary antibodies overnight at 4°C. Subsequently, the PVDF membranes were washed three times with Tris-buffered saline with Tween 20 (TBST), incubated with secondary antibodies for 1 hour at room temperature, and finally subjected to visualization.

Animal Grouping

Male Sprague-Dawley (SD) rats (body weight: 250 ± 20 g) were provided by the Animal Experimentation Center of Wenzhou Medical University. All rats were randomly divided into 5 groups (n=10 per group): Sham operation (Sham) group, middle cerebral artery occlusion/reperfusion (MCAO/R) group, IMP group, IMP@HMSNs group, and NCM/IMP@HMSNs group. For the Sham group, only the External Carotid Artery (ECA) and Common Carotid Artery (CCA) were dissected without nylon monofilament suture insertion. One hundred and twenty minutes after surgery, sterile normal saline (1 mL/kg) was administered via the sublingual vein. For the MCAO/R group, after 120 minutes of ischemia, sterile normal saline (1 mL/kg) was given via the sublingual vein at the time of reperfusion. For the IMP group,

IMP@HMSNs group, and NCM/IMP@HMSNs group, after 120 minutes of ischemia, the corresponding drugs were administered via the sublingual vein at the time of reperfusion (drug concentration calculated based on the IMP component, 2 mg/kg, 1 mL/kg). From the day of model establishment, the body weight changes of the rats were recorded daily.

Establishment of the Middle Cerebral Artery Occlusion/Reperfusion (MCAO/R) Model

After isoflurane gas anesthesia, the rats were shaved at the cervical region, placed in a supine position, with the neck fully exposed and disinfected. A midline cervical incision was made, and subcutaneous tissues and fat were bluntly dissected. Under a stereomicroscope, the right Common Carotid Artery (CCA), Internal Carotid Artery (ICA), and External Carotid Artery (ECA) were carefully separated. Care was taken to avoid the vagus nerve to prevent respiratory depression in rats due to injury. A small incision was made at the distal end of the ECA, and a nylon monofilament suture was inserted along the direction of the CCA to the bifurcation of the CCA, ICA, and ECA. The ECA was transected at the distal end, and the residual ECA stump was rotated 180° around the bifurcation to allow the suture to enter the distal ICA at an appropriate angle. When the marked black dot reached the bifurcation, suture insertion was stopped and timing was initiated. The insertion depth of the suture was approximately 18–20 mm, at which point the suture just entered the intracranial Anterior Cerebral Artery, occluding the opening of the Middle Cerebral Artery, reducing blood flow in brain tissue, and causing hypoxia-ischemia. Reperfusion was performed after 120 minutes of ischemia. At 120 minutes after suture insertion, the suture was pulled out by approximately 1 cm, retracting the hemispherical tip of the suture toward the proximal end. At this time, blood flow to the Middle Cerebral Artery was restored, and blood reperfusion occurred in the hypoxic-ischemic brain tissue. The wound was sutured layer by layer carefully. After suture, the skin was disinfected with povidone-iodine, and bleeding was checked. The animals were returned to cages with attention to postoperative warmth preservation.

In vivo Targeting Validation

The accumulation of NCM/IMP@HMSNs in the brains of MCAO/R model rats was monitored using the IVIS Lumina Series III small animal in vivo optical imaging system. MCAO/R models were established, and a single dose of DIR-labeled NCM/IMP@HMSNs was administered via the tail vein 24 hours after reperfusion. Twenty-four hours after injection, the rats were sacrificed, and the brain tissues were excised and prepared into coronal sections for fluorescence imaging. Visualization was performed using the IVIS imaging system to observe the targeting of NCM/IMP@HMSNs to the injured hemisphere in MCAO/R model rats.

Protective Effects of Each Treatment Group on the MCAO/R Model

The success of the rat MCAO/R model was verified by performing neurological deficit scoring on rats 24 hours after cerebral ischemia-reperfusion, combined with brain scanning and imaging via magnetic resonance imaging (MRI). The infarct volume of rats was evaluated based on MRI results, and the degree of edema in the affected side was observed. Motor and sensory neurological functions were assessed via neurological deficit scoring, while spatial cognition and memory functions were evaluated using the Morris water maze test.

Neuroprotective Effect Study in vivo

On Day 10 after ischemia-reperfusion, 6 rats from each group were euthanized, and their brains were removed. The fresh brain tissues were placed in pre-chilled Petri dishes and immediately stored at −80°C refrigerator for subsequent use. Additionally, blood samples were collected from abdominal aorta or orbital sinus for serum biochemical analysis. Furthermore, 3 rats from each group were anesthetized, and the right atrial appendage was incised. Pre-chilled normal saline was perfused through the left ventricular apex until the liver turned khaki, followed by perfusion with 4% paraformaldehyde. Severe twitching of the rats' limbs observed at the start of perfusion was a sign of successful perfusion of the perfusate into the brain. After perfusion, the heads were severed to remove the brains, which were

then placed in centrifuge tubes containing 35 mL of 4% paraformaldehyde and fixed for 48 hours. Hematoxylin-eosin (HE) staining, Nissl staining, and immunohistochemistry were performed subsequently.

Determination of Antioxidant Enzyme and Peroxide Levels

The injured cerebral cortical tissue was excised, and the fresh brain tissue was weighed accurately. Pre-chilled 0.9% normal saline (9 volumes) was added at a weight (g): volume (mL) ratio of 1:9. The mixture was placed in a pre-cooled cryogenic grinder for mechanical homogenization to prepare a 10% brain tissue homogenate. Lactate dehydrogenase (LDH), glutathione (GSH), total superoxide dismutase (T-SOD), malondialdehyde (MDA), and catalase (CAT) were determined according to the manufacturer's instructions of the corresponding kits.

Statistical Methods

Data were analyzed using SPSS 22.0 statistical software, and graphs were generated with GraphPad Prism 7.0 and Origin 2021 plotting software. All data were expressed as mean ± standard deviation ($\bar{x} \pm SD$). For quantitative data conforming to normal distribution, pairwise comparisons among multiple groups were performed using one-way analysis of variance (ANOVA). Data not conforming to normal distribution were analyzed by nonparametric tests. A P value < 0.05 was considered to indicate a statistically significant difference.

Results

Synthesis and Characterization of HMSNs

The particle size and zeta potential of the HMSNs were determined using a Malvern Zetasizer Nano ZS 90 laser nanoparticle sizer. As shown in Figure 1A, the particle size was concentrated at 153.1 nm, and the PDI was 0.049, which indicated that the HMSNs had a relatively homogeneous particle size with a normal distribution and a narrower distribution range. As shown in Figure 1B, the potential of the prepared HMSNs was −48.8 mV, and the absolute value was around 50 mV, reflecting that the HMSNs had better stability and dispersion.

The 3D images of the sample surface were obtained by SEM, and the results are shown in Figure 1C, from which it can be observed that the prepared HMSNs nanoparticles are basically regular spherical, with uniform size, good dispersion, but poor monodispersity. It may be due to the fact that HMSNs have a very large specific surface area, the difference between the total number of atoms and the number of atoms on the surface is large, and the lack of neighboring atoms around the surface atoms is unsaturated, which makes it easy to combine with other

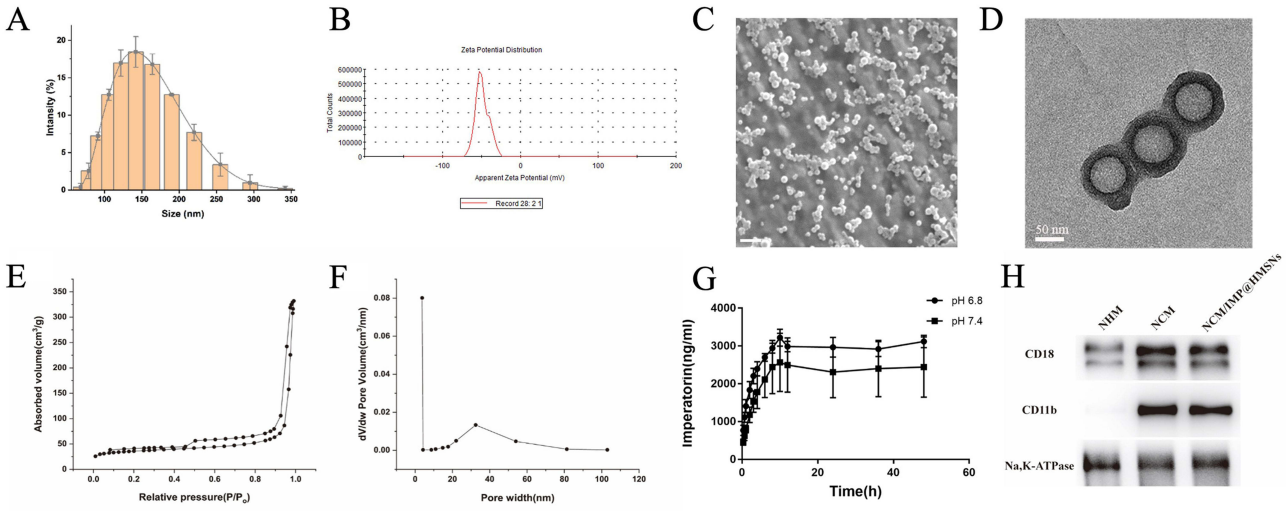

Figure 1 Characterization of HMSNs. (**A**) Particle Size Distribution. (**B**) Zeta Potential Distribution. (**C**) Scanning Electron Microscopy (SEM). (**D**) Transmission Electron Microscopy (TEM). (**E**) Nitrogen Adsorption-Desorption Characterization. (**F**) Pore Size Distribution. (**G**) Drug Release Curves of IMP@HMSNs in pH 6.8 and pH 7.4 Buffer Solutions. (**H**) Detection of the Expression of Cell Membrane Surface Markers on Differentiated HL60 Cells.

https://doi.org/10.2147/IJN.S592970

atoms to form a stable structure, and the aggregation of a single HMSN is easy to occur. TEM was used to obtain the internal structure images of the samples, and the results are shown in Figure 1D. It can be observed that the HMSNs have a regular spherical shell structure, the average particle size is about 143.46 nm, the average inner diameter of the hollow portion is 87.94 nm. The average thickness of the silica spherical shell is about 25.66 nm, which makes the thickness of the spherical shell more uniform. After analyzing the above TEM and SEM results, it is inferred that the prepared HMSNs have uniform wall thickness and particle size and good drug loading properties.

Nitrogen Adsorption-Desorption Characterization of HMSNs

The surface adsorption characteristics of HMSNs were determined by the BET specific surface area method, and the results are shown in Figure 1E. The nitrogen adsorption isothermal curves belonged to the Langmuir type IV according to the classification standard of the IUAPC. The curves had the mesoporous hysteresis loop, which was a characteristic feature of mesoporous structure, indicating that the HMSNs had a nano-mesoporous structure. Based on the nitrogen adsorption-desorption curves, the pore size distribution curves were obtained by applying the BJH model (Figure 1F), and the maximum value corresponded to the mesoporous pore size of HMSNs, which was 29.05 nm.

Drug Loading and Drug Release Assays

According to the HMSNs component concentration meter, the weights of HMSNs before and after loading IMP at the same concentration were accurately weighed. The LC% of HMSNs to IMP was calculated to be 32.71%, and the EE% was 31.84%. In the drug release experiments, plot the drug release curves of IMP@HMSNs in pH 6.8 and pH 7.4 buffer solutions, and the results are shown in Figure 1G. After 12 hours of dialysis, the release of IMP reached equilibrium, and the concentration remained basically the same.

Expression of Surface Markers of HL60 Membrane

The expression of CD18 and CD11b in undifferentiated HL60 cell membranes (NHM), differentiated HL60 cell membranes (NCM), and cell membranes extracted from prepared NCM/IMP@HMSNs were detected by Western blot method, and the results are shown in Figure 1H. The expression of CD18 and CD11b on the surface of HL-60 cells was significantly increased after differentiation by DMSO. The expression of CD11b on the surface of undifferentiated HL-60 cells was basically absent, but the expression was significantly increased after differentiation by DMSO. This suggests that the expression of CR3 on the surface of HL-60 cells is greatly increased after differentiation by DMSO, and it is inferred that NCM can exhibit NCM-like inflammatory chemotaxis and deliver drugs to the site of inflammation. In addition, the negative expression of calnexin in Figure S1 confirms the absence of intracellular contamination in the extracted membrane.

Drug Uptake of HMSNs in SH-SY5Y Cells

Prior to this, we have verified that HMSNs and IMP at various concentrations exhibit favorable biocompatibility and stability in SH-SY5Y cells, respectively (Figure S2A and B). In the intracellular drug uptake assay of HMSNs in SH-SY5Y cells, the results were shown in Figure 2A. Both rhodamine B loaded by HMSNs and NCM coated by the outer layer could be uptaken by the SH-SY5Y cells. Rhodamine B was mainly distributed in the cytoplasm after uptake, and NCM was incorporated into the cell membrane after being uptaken. It is suggested that the drug-loaded MSNs, which can release the drug in the culture medium and be taken up by the cells, NCM/IMP@HMSNs may enter the cells by cytosolization, and the carrier of HMSNs as the core releases the loaded drug inside the cells after cell entry, which is beneficial for the nanocarriers to deliver the drug to the site of inflammation in vitro in a targeted manner and to release it, which can be taken up by the specific cells to exert the therapeutic effect.

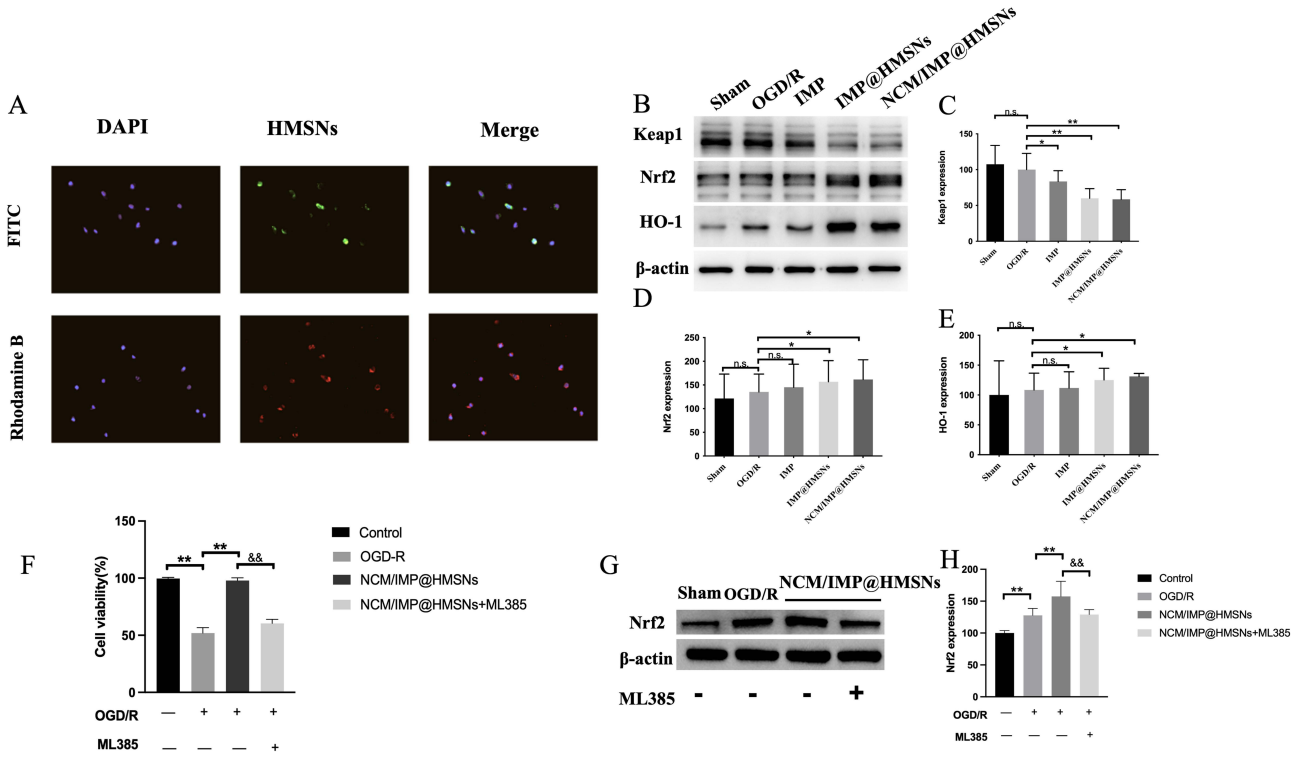

Figure 2 Biomimetic NCM/IMP@HMSNs delivery system protective effects against OGD/R induced injury in SH-SY5Y cells. (**A**) Uptake Behavior of NCM/IMP@HMSNs in SH-SY5Y Cells. (**B**) Western Blot of the Effects of Each Treatment Group on the Nrf-2/ARE/Keap1 Pathway in SH-SY5Y Cells After OGD/R. (**C–E**) Bar Graph of the Relative Expression Levels of Keap1, Nrf2 and HO-1 Protein Among Different Groups. (**F**) Cell viability. (**G** and **H**) Nrf2 Protein Expressions in Each Group after ML385 Treatment. n.s., no significance, $^{*}p < 0.05$, $^{**}p < 0.01$, vs. OGD/R group; $^{\&\&}p < 0.01$, vs. NCM/IMP@HMSNs group.

Effects of NCM/IMP@HMSNs on the Nrf2/ARE/Keap1 Pathway in SH-SY5Y Cells After OGD/R

After OGD/R, IMP effectively improved the viability of SH-SY5Y cells (Figure S2C). Protein expression levels of the Nrf2/ARE/Keap1 pathway were detected by Western Blot, and the results are shown in Figure 2B–E. Compared with normally cultured cells, the Keap1 protein level in SH-SY5Y cells was downregulated to varying degrees 24 h after OGD/R. In contrast to the OGD/R group, co-culture with different forms of IMP during reoxygenation significantly downregulated the Keap1 protein level. There was no significant difference in Keap1 protein expression between the IMP@HMSNs group and the NCM/IMP@HMSNs group, and both were significantly lower than that in the IMP group. Whether the nanocarrier is coated with a biomimetic cell membrane (NCM) has little impact on this promotional effect. Compared with normally cultured cells, the Nrf2 protein level in SH-SY5Y cells was upregulated to varying degrees 24 h after OGD/R. Compared with the OGD/R group, co-culture with different forms of IMP during reoxygenation significantly upregulated the levels of Nrf2 protein and its downstream HO-1 protein. The Nrf2 protein level in the IMP@HMSNs group was significantly higher than that in the IMP group, while there was no significant difference in Nrf2 protein level between the IMP@HMSNs group and the NCM/IMP@HMSNs group. After co-culture with IMP, the change trend of the downstream HO-1 protein level was consistent with that of the Nrf2 protein level.

To verify the pivotal role of Nrf2 in mediating the neuroprotective effect of NCM/IMP@HMSNs, SH-SY5Y cells were co-treated with ML385, a selective Nrf2 inhibitor. After OGD/R, NCM/IMP@HMSNs markedly elevated cell viability as shown in Figure 2F. This protective effect was substantially reversed upon ML385 intervention. Meanwhile, ML385 downregulated Nrf2 protein expression (Figure 2G and H), demonstrating that the neuroprotection exerted by NCM/IMP@HMSNs relies on Nrf2 activation.

https://doi.org/10.2147/IJN.S592970

In vivo Targeting of NCM/IMP@HMSNs

The inflammatory response caused by ischemia/reperfusion can guide the NCM/IMP@HMSNs with neutrophil membrane characteristics to actively target the site of brain damage. DIR-labeled NCM/IMP@HMSNs were injected into mice through the tail vein, and then the brains were taken out for fluorescence imaging in the coronal section at 24 h. The results are shown in Figure 3A, which indicates that DIR-labeled NCM/IMP@HMSNs have strong fluorescence in the ischemic side of the brain hemisphere, and are enriched in the damaged brain tissue. The validation of the in vivo targeting of NCM/IMP@HMSNs suggests that the NCM coated with nanocarriers can allow drug-carrying nanoparticles to be targeted to the site of inflammation in the brain and be enriched at the site of injury, so that the NCM/IMP@HMSNs could be delivered to the site of inflammation and released by specific release and absorption by targeted cells to achieve therapeutic effects.

NCM/IMP@HMSNs Amelioration of MCAO/R-Induced Infarct Volume

The cerebral infarction status of rats in each group is shown in Figure 3B. In the Sham group, no high-intensity signals were observed in brain tissues at different levels, and no obvious infarct areas were detected. In the MCAO/R group, distinct infarct areas were visualized at all levels; at −1.5 mm from the bregma, the entire ischemic hemisphere exhibited

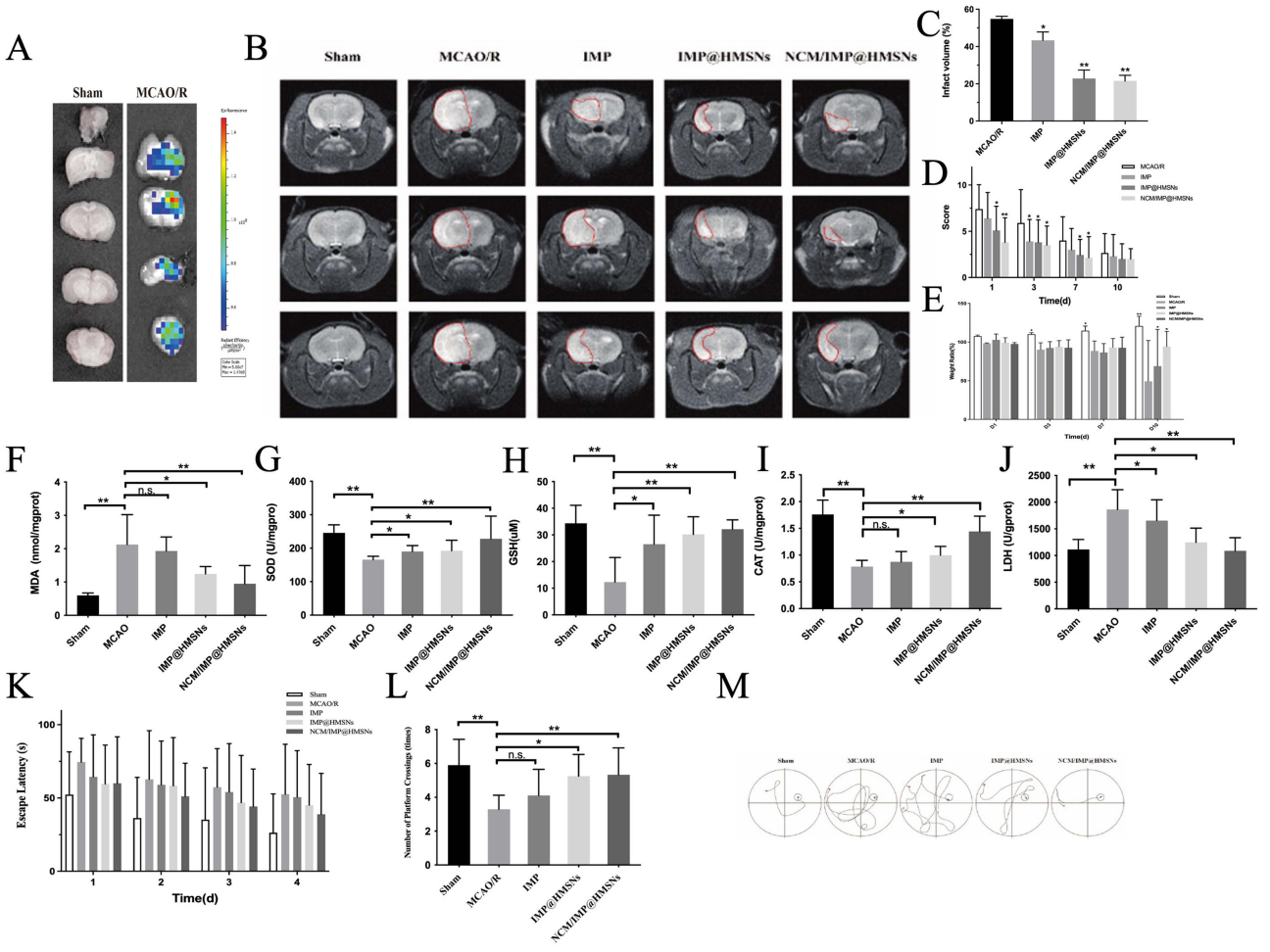

Figure 3 Neurofunctional improvement in MCAO/R rats across different treatment groups. (**A**) Whole-Brain Distribution Behavior of DIR-Labeled NCM/IMP@HMSNs. (**B**) MRI Images After MCAO/R. (**C**) Bar Graph of Infarct Volume Ratio. (**D**) Neurobehavioral Function Scoring. (**E**) Body Weight Changes. Effects of Each Treatment Group on the Antioxidant Capacity of Brain Tissue. (**F**) Effects of different treatment groups on MDA in brain tissue. (**G**) Effects of different treatment groups on SOD in brain tissue. (**H**) Effects of different treatment groups on GSH in brain tissue. (**I**) Effects of different treatment groups on CAT in brain tissue. (**J**) Effects of different treatment groups on LDH in brain tissue. (**K**) Comparison of Escape Latency of Rats in Each Group. (**L**) Comparison of the Number of Platform Crossings of Rats in Each Group. (**M**) Representative Swimming Trajectories of Rats in Each Group on Day 4. n.s., no significance, $*p < 0.05$, $**p < 0.01$, vs. MCAO/R group.

https://doi.org/10.2147/IJN.S592970

high-intensity signals, with significant infarction and midline shift. Compared with the model group, the infarction status of rats in each administration group was alleviated to varying degrees. Free IMP intervention had a limited effect on reducing the cerebral infarct area of rats, but the T2 signal intensity was significantly weakened and no midline shift occurred, suggesting that IMP may reduce the edema severity of ischemic brain tissues. After treatment with IMP@HMSNs and NCM/IMP@HMSNs, the T2 signal of the ischemic hemisphere was significantly reduced, the cerebral infarct area of rats was remarkably decreased, and NCM/IMP@HMSNs exhibited a significant advantage. Compared with the MCAO/R group, the corresponding cerebral infarct area in each administration group was also significantly improved, and the effect of NCM/IMP@HMSNs on ameliorating infarct volume was more prominent (Figure 3C).

NCM/IMP@HMSNs Improves Neurobehavioral Function of Rats

We prepared a rat model of focal cerebral ischemia using the middle cerebral artery suture-occlusion method. Focal ischemia models mostly caused sensory and motor dysfunction, and whole-brain ischemia models caused significant cognitive and memory dysfunction. We used the modified mNSS to assess the degree of neurological damage in each group of rats at 24 h, 3 d, 7 d and 10 d after reperfusion. As shown in Figure 3D, compared with the MCAO/R group, IMP@HMSNs and NCM/IMP@HMSNs significantly reduced the mNSS scores of the rats after 24 h reperfusion, and NCM/IMP@HMSNs was significant. The mNSS scores of the rats in the groups decreased gradually with time, and there was no statistically significant difference in the mNSS scores between the groups on the 10th day of reperfusion. The mNSS scores were not statistically different from those in the MCAO/R group. The results of the mNSS scores suggested that cerebral ischemia-reperfusion injury caused impaired neurobehavioral ability in rats, and the intervention with NCM/IMP@HMSNs could alleviate the degree of impaired neurobehavioral ability.

NCM/IMP@HMSNs Improves Changes in Body Mass Index

The body weights of rats in each group were weighed and recorded on days 1, 3, 7 and 10 before and after reperfusion, respectively, and the body mass index was calculated and plotted as a histogram of body weight variations. As shown in Figure 3E, the body mass index of the Sham group increased steadily over time, and the sham operation did not significantly affect the Sham rats, while the body mass index of the rats in all groups after reperfusion decreased steadily over time, which was analyzed to be due to the fact that the damage caused by the reperfusion had affected the overall state of the rats, resulting in the decrease in body mass. Compared with the rats in the MCAO/R group, the Body Mass Index (BMI) of rats in all drug-dosing groups decreased to different degrees, and the trend of BMI in all groups was consistent with the results of the mNSS scores, which suggests that the neurological impairment caused by reperfusion affects the feeding behaviors and the overall vitality of the rats, and their health status is impaired. The BMI results suggest that cerebral ischemia/reperfusion injury causes weight loss in rats, and that intervention with NCM/IMP@HMSNs can alleviate the BMI loss induced by ischemia/reperfusion injury.

NCM/IMP@HMSNs Enhances the Antioxidant Capacity of Brain Tissue

It was found that SOD, GSH and CAT antioxidant enzymes decreased after MCAO injury, and SOD, GSH and CAT increased after IMP@HMSNs treatment, and the results are shown in Figure 3F–J. After ischemia-reperfusion injury, the MDA and LDH level of brain tissue increased significantly. The MDA and LDH level decreased significantly after NCM/IMP@HMSNs intervention. The results suggest that NCM/IMP@HMSNs can significantly increase the level of antioxidant enzymes and decrease the level of lipid peroxides in the damaged brain tissues after ischemia-reperfusion injury in rats.

NCM/IMP@HMSNs Enhances Learning and Memory Abilities of Rats

The rats were allowed a short period of wound recovery for the first two days after reperfusion to prevent factors such as inadequate wound healing or contact with water from interfering with the findings. We conducted the water maze experiment for 5 consecutive days starting from the 3rd day of reperfusion, at which time all the wounds of the rats had begun to scab and recovered, and the rats were able to raise their heads and walk freely without being affected by the

 https://doi.org/10.2147/IJN.S592970

pulling of the wounds. The results of the first 4 days of localization and navigation experiments are shown in Figure 3K. Compared with the Sham group, the escape latency of rats in the MCAO/R group was significantly prolonged by ischemia/reperfusion, but there was no significant change in the swimming speed, so we can initially rule out the prolongation of the escape latency due to the limb movement disorders of the rats. Compared with the model group, the escape latency of rats in all drug dosing groups was shortened to different degrees, and the use of IMP monomer did not significantly shorten the escape latency, but the time required to search for a hidden platform was significantly shorter in the rats treated with IMP@HMSNs and NCM/IMP@HMSNs. The escape latency of rats in all groups shortened as the training time went on.

After the platform was removed on the fifth day, the number of rats crossing the platform area was observed in each group, and the results were shown in Figure 3L. Compared with the Sham group, the number of rats crossing the platform in the MCAO/R group was significantly reduced, while compared with the MCAO/R group, the number of rats crossing the platform area was increased to different extents in each drug dosing group, and there was a significant increase in the number of rats crossing the platform area after the interventions of using IMP@HMSNs and NCM/IMP@HMSNs. The representative swimming trajectories of rats in each group on the last day of the localization navigation experiment are shown in Figure 3M. It can be seen that the length of the paths taken by rats in the Sham group and the NCM/IMP@HMSNs group to search for platforms was significantly shorter compared with those in the MCAO/R group, and there was no significant change in the length of the paths taken by rats in the IMP group to search for hidden platforms compared with those in the MCAO/R group. IMP@HMSNs group rats had a significantly shorter path length. This suggests that rats in the sham-operated group have better learning memory ability, but in rats with ischemia-reperfusion injury, this spatial learning memory ability is impaired. The rats in the IMP@HMSNs group and the NCM/IMP@HMSNs group gradually recovered their spatial memory ability during continuous training, suggesting that the intervention with NCM/IMP@HMSNs can improve the learning memory ability in rats with ischemia-reperfusion injury.

Effects of Each Treatment Group on Brain Tissue Morphology in MCAO/R Model Rats

All treatment groups exhibited negligible systemic toxicity, and no obvious histopathological lesions were observed in major organs (Figures S3 and S4). The results of HE staining of brain tissue sections are shown in Figure 4A. The brain tissue of rats in the Sham group was structurally normal, the cells were arranged in a close and orderly manner, the morphology was normal, the nuclei of the cells were rounded and large, the cytoplasm was uniformly stained, and the tissue did not have any significant necrosis or infiltration. In the MCAO group, the brain tissue of rats showed extensive infarction, with the infarcted area showing a skeletonized reticular structure, disorganized cell arrangement, irregular cell morphology, shrunken nuclei, deep staining of cytoplasm. Compared with the MCAO/R group, the brain tissue damage of rats in each drug-dosing group was alleviated to different degrees. In the IMP group, the cell damage was reduced, the tissue arrangement was disorganized, but the degree of disorganization and the degree of nuclear consolidation was slightly lower than that of the MCAO/R group; in the IMP@HMSNs group and the NCM/IMP@HMSNs group, the brain tissue damage was alleviated to a good extent, with the cell arrangement being relatively tightly organized, the cellular morphology tending to be normalized, the number of pyknotic nuclei was decreased to a certain extent.

The results of Nissl staining of brain tissue sections are shown in Figure 4B, the neuronal Nissl bodies in Sham group were abundant and regular in shape, while the number of Nissl bodies in MCAO/R group was reduced in degeneration and solidification; the morphology of Nissl bodies in the injured area of brain tissue of rats tended to be normalized and their number was increased after the interventions of IMP@HMSNs and NCM/IMP@HMSNs. The effect of NCM/IMP@HMSNs was better than that of IMP@HMSNs, and the morphology of Nichols' bodies in the injured area of rat brain tissue became rounded and enlarged, suggesting that the number of neurons surviving after ischemia/reperfusion injury was reduced and the function of nerve cells was lowered, and that the NCM/IMP@HMSNs intervention was able to protect neurons injured in ischemia/reperfusion injury and reduce neuronal apoptosis.

Protective Effect of NCM/IMP@HMSNs on the Injured Brain

The protein expression levels of Nrf2/ARE/Keap1 pathway in the brain injury area of rats in each group were detected by Western Blot method, and the results are shown in Figure 4C. Compared with Sham group, Keap1 protein levels were

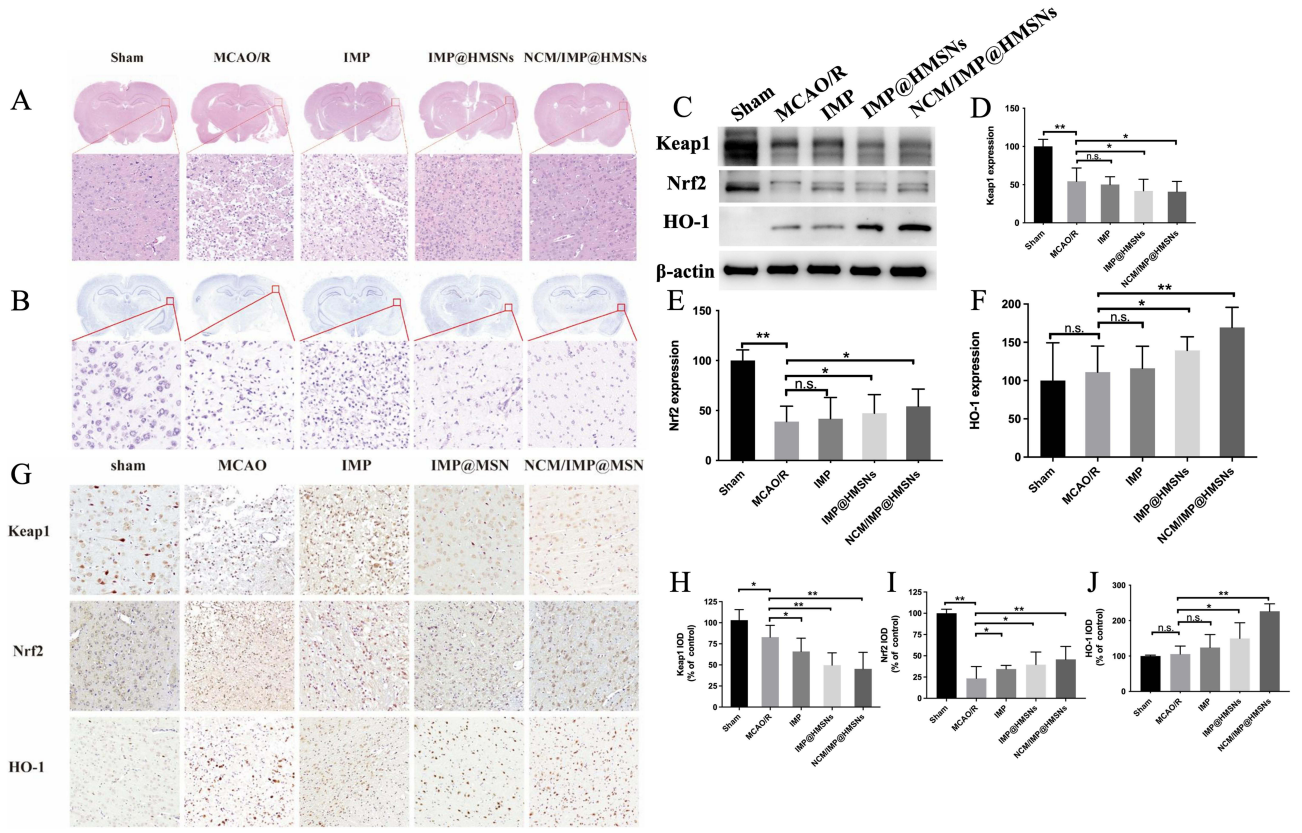

Figure 4 Antioxidant protective effects of different treatment groups on brain tissue of MCAO/R model rats (**A**) Representative Images of HE-Stained Brain Tissue Sections in Each Group. (**B**) Representative Images of Nissl-Stained Brain Tissue Sections in Each Group. (**C**) Western Blot Bands of the Nrf2/ARE/Keap1 Pathway in the Brain Injury Area of Rats in Each Group. (**D–F**) Bar Graph of the Relative Expression Level of Keap1, Nrf2 and HO-1 Protein Among Different Groups. (**G**) Immunohistochemical Images of Nrf2/ARE/Keap1 Pathway Proteins in the Cerebral Cortex of Rats in Each Group. (**H–J**) Bar Graph of Keap1, Nrf2 and HO-1 IOD Among Different Groups. n.s., no significance, **p* < 0.05, ***p* < 0.01, vs. MCAO/R group.

down-regulated to different degrees in the brain tissues of rats injured by ischemia/reperfusion; compared with the MCAO/R group, Keap1 protein levels were down-regulated in all groups, and the most advantageous was in the NCM/IMP@HMSNs intervention, with Keap1 protein expression levels significantly lower than those in the MCAO/R group (Figure 4D). Compared with the Sham group, the levels of Nrf2 protein in the damaged areas of the brain after ischemia/reperfusion were down-regulated to different degrees, which may be due to the fact that the ubiquitination degradation of Nrf2 induces the production of free Nrf2 in the cytoplasm, and at the same time, the newly produced Nrf2 dislocation to the nucleus of the cell to enhance the expression of ARE and HO-1, which leads to the decrease of cytoplasmic levels of Nrf2 (Figure 4E). Compared with the MCAO/R group, the levels of Nrf2 protein and HO-1 protein in the downstream region were significantly up-regulated in all the drug-dosing groups, and the levels of Nrf2 protein were significantly higher in the IMP@HMSNs group and the NCM/IMP@HMSNs group than in the MCAO/R group, which indicated that there was a significant advantage of the NCM/IMP@HMSNs intervention (Figure 4F). The increase of HO-1 protein level in the downstream region after the intervention of each administration group was consistent with the trend of Nrf2 protein level.

Immunohistochemistry

Immunohistochemical staining was used to detect the expression of Nrf2/ARE/Keap1 pathway proteins in the cortical area of rats, and the immuno-positive substance were displayed as brown dots or granules, the results of which are shown in Figure 4G, and the results of IOD values of the proteins were analyzed in Figure 4H–J, respectively. After ischemia/reperfusion injury in MCAO/R rats, the morphology of brain tissue at the edge of the infarct foci was consistent with the pathological changes characteristic of infarction, and the expression level of Keap1 protein in the damaged cortex was

https://doi.org/10.2147/IJN.S592970

reduced. The expression of Keap1 protein in the damaged cortical area was reduced to different degrees in all groups, and the trend of Keap1 expression in all groups was consistent with the WB results. Compared with the Sham group, the expression of Nrf2 protein in the damaged cortical area of rats in the MCAO/R group after ischemia-reperfusion injury was significantly decreased, and the decrease of Nrf2 expression level was mitigated to a different extent in all the groups, and the expression level of Nrf2 in the cortical area of rats in the NCM/IMP@HMSNs group tended to be closer to that in the Sham group. After ischemia-reperfusion injury, the expression level of HO-1 increased significantly in all groups of rats, and the highest expression level of HO-1 in the damaged cortex in the NCM/IMP@HMSNs group, which was in agreement with the WB results.

Discussion

Stroke, as a major chronic non-communicable disease that poses a serious threat to human health, is induced by multiple factors such as hypertension, blood glucose, cholesterol, body mass index, smoking, physical activity and diet.[27,28] Furthermore, the necessity of alleviating ischemic stroke reperfusion injury urgently needs to be further addressed.[29]

HMSNs with a particle size of about 150 nm were prepared by the improved Stoer method with good dispersion, and their mesoporous hollow structure was determined by TEM, which laid the basic structure for subsequent drug loading. The prepared HMSNs were loaded with IMP (IMP@HMSNs), and the drug loading rate was determined to be 31.84%, and they were coated with bionic cell membrane, and NCM/IMP@HMSNs were prepared, and it was verified that the prepared HMSNs were in accordance with the needs. The in vitro drug release profiles of IMP@HMSNs were determined, and IMP@HMSNs released more in buffer solution at pH 6.8, which was more favorable for the release of drugs from the HMSNs-loaded IMP drug delivery platform in an acidic environment. HL-60 cells can exhibit neutrophil-like properties after differentiation,[30] and thus HL-60 cell membranes were chosen to encapsulate prepared HMSNs were coated with HL-60 cell membranes. Neutrophils can sense and move to the site of inflammation, and the use of NCM-like coated nanoparticles not only enhances targeted drug delivery through this inflammatory chemotaxis ability, but also helps to evade immune clearance.[31] Neutrophils adhere to activated endothelial cells via adhesion proteins on the membrane surface, and leukocytes express a variety of specific adhesion molecules integrins on the surface, with β2-integrins predominating, including LFA-1, CR3 and CR4.[32,33] The β2-integrin consists of two parts, the α-subunit and the β-subunit. The β-chain of LFA-1, CR3, and CR4 is CD18, also known as Integrin β2, while the α-chain is different, CD11a, CD11b, and CD11c, respectively.[34] Complement receptor type III (CR3), also known as Mac-1, is a heterodimeric glycoprotein composed of two peptide chains, the α-chain (CD11b) and the β-chain (CD18), bound by a noncovalent bond, which mediates the adhesion of neutrophils to the endothelium during the inflammatory response.[35] DMSO-induced HL-60 cells were verified by Western-Blot assay, and the neutrophil membrane surface markers CD18 and CD11b were highly expressed in the induced cell membranes, but were not expressed in the membranes of uninduced HL-60 cells, so theoretically, the membranes of DMSO-induced HL-60 cells have a function similar to that of inflammatory chemotaxis of neutrophils.

Although neutrophil membrane-coated nanoparticles exhibit favorable inflammatory targeting capacity, relevant safety concerns remain to be elaborated. Firstly, the neutrophil membranes derived from HL-60 cells originate from leukemic cell lines, whose surface protein profiles may differ abnormally from primary human neutrophils.[36] Secondly, despite the inflammatory tropism facilitating lesion targeting, it may theoretically cause non-specific accumulation at multiple inflammatory loci, especially in patients suffering from systemic inflammatory disorders.[37] Furthermore, inherent heterogeneity of cell-derived membranes has been well documented in exosome research. Variations in protein expression patterns among different batches could substantially affect therapeutic efficacy and biosafety.[38] Notably, the current study only focuses on local cerebral ischemic injury models without involving systemic inflammatory conditions, and relevant safety verification under complex pathological backgrounds needs further exploration. In addition, although HL-60 cells are immortalized, practical challenges still exist in maintaining membrane integrity during storage and achieving large-scale production. Repeated freeze-thaw cycles and long-term storage at suboptimal temperatures can impair membrane protein stability and weaken the therapeutic efficacy of nanoparticles. These hurdles greatly hinder the clinical translation and practical application of HL-60-derived biomimetic materials.

Nrf2 is a positive regulator of human ARE and plays a crucial role as an important endogenous antioxidant receptor in the cellular antioxidant defense system.[39,40] Nrf2 regulates the expression of antioxidant proteins such as quinone oxidoreductase (NQO1), glutathione sulfotransferases (GSTs), Glutamyl cysteine ligase (GCLCs), and HO-1 by binding to AREs in the nucleus. Under normal conditions, Nrf2 binds to Keap1 in the cytoplasm and is rapidly degraded by the ubiquitin proteasome. Oxidative stress or stimulation by nucleophilic substances may trigger the dissociation of Nrf2 from Keap1 to release free Nrf2 and diminish the ubiquitination and subsequent degradation of Nrf2, while increasing the ubiquitination and degradation of Keap1 to allow for the accumulation of Nrf2 in the cell. Free Nrf2 dislocated from the cytoplasm to the nucleus to bind to the ARE and trigger the expression of downstream antioxidant proteins. In this experiment, we successfully replicated the OGD/R of SH-SY5Y cells, and determined the concentration (10 μM) at which IMP was co-incubated with cells after OGD/R injury. Preliminary WB analysis confirmed that NCM/IMP@HMSNs exerts a neuroprotective effect on OGD/R-injured SH-SY5Y cells in vitro via the Nrf2/ARE/Keap1 pathway. It is superior to the direct use of IMP at the same dose, as it activates the downstream of the signaling pathway to induce higher expression of HO-1 protein, thereby exerting a stronger antioxidant effect.

In vivo, NCM/IMP@HMSNs were enriched in the damaged brain tissues. The preparation of nanocarriers coated with NCM with neutrophil characteristics could enable the drug-carrying nanoparticles to target the inflammation sites of brain injury and enrich the drug at the injury sites. The infarcted area of the rat brain was verified by MRI T2 imaging, and there were differences in the area of infarcts that could be improved by different drug interventions, and the most obvious effect was observed in the NCM/IMP@HMSNs group. The modified mNSS score was used to assess the degree of neurological deficits of rats in each group, and the mNSS score after 24 h reperfusion was significantly reduced in the IMP@HMSNs and NCM/IMP@HMSNs groups, with the most obvious effect in the NCM/IMP@HMSNs group. The effect of NCM/IMP@HMSNs was the most obvious, and with the passage of time, the rats in each group gradually recovered their neurological functions, and the scores were lower than those of the other groups with no significant difference.

We used the Morris water maze test to evaluate the effect of NCM/IMP@HMSNs on spatial learning and memory function in MCAO rats. Changes in cognitive function after stroke have emerged as a research hotspot, and the assessment of spatial cognitive function is a commonly used method in experimental studies. The Morris water maze test is mainly employed to evaluate the spatial learning and memory abilities of rodents. Rats learn to locate a hidden platform at a fixed position through daily standardized swimming training, forming stable spatial location cognition. The hippocampal cortical pathway and dorsal striatum play key roles in regulating spatial memory.[41,42] In the water maze test, an intact hippocampus is a prerequisite for rats to successfully establish spatial location cognition. The focal cerebral ischemia model used in our study generally does not cause damage to the hippocampal structure, so MCAO/R rats can still gradually establish spatial location cognition through training.

The results of HE and NISSL staining showed that NCM/IMP@HMSNs could reverse the pathological changes of infarcted area after ischemia/reperfusion, protect neuronal cells, and reduce apoptosis of neuronal cells. Through Western-Blot and immunohistochemical staining, it was clear that NCM/IMP@HMSNs could play an antioxidant role by activating the Nrf2/ARE/Keap1 pathway and regulating the expression of downstream antioxidant proteins, and that the effects of NCM/IMP@HMSNs on the expression of Nrf2/ARE/Keap1 pathway proteins were mainly concentrated in the infarcted area and the surrounding cortex. It has been reported that IMP exerts a bidirectional regulatory effect on the Nrf2/ARE/HO-1 pathway. In the early stage of the disease, IMP alleviates the inflammatory response by promoting the expression of Nrf2, ARE, and HO-1; its effect on the Nrf2/ARE/HO-1 pathway is significantly weakened in the middle stage; in the late stage, it reduces inflammation by inhibiting the expression of Nrf2, ARE, and HO-1. After the disease stabilizes and progresses to the late stage, the determination of protein expression levels of the Nrf2/ARE/HO-1 pathway may differ from those in the early stage of the disease. Subsequent experiments can further explore the mechanism of action exerted at different stages of the disease.

Conclusion

In this study, we successfully synthesized HMSNs nanoparticles with a regular hollow mesoporous structure, loaded them with IMP, a natural coumarin with anti-inflammatory activity, and coated the surface with a biomimetic cell

membrane to construct the NCM/IMP@HMSNs nano-delivery system. This nano-delivery system improves bioavailability and metabolic stability, and can accumulate in cerebral ischemia-reperfusion damaged regions. In vitro experimental results demonstrated that NCM/IMP@HMSNs can be internalized and utilized by cells in vitro, exerting a potent antioxidant effect on the OGD/R-induced SH-SY5Y cell model. In vivo studies revealed that the NCM/IMP@HMSNs drug delivery system can effectively accumulate the ischemia-reperfusion brain injury area in MCAO/R rats and regulate oxidative stress at the injured site via the Nrf2/ARE/Keap1 signaling pathway, which is beneficial for neural recovery after ischemia-reperfusion. In conclusion, our research provides a promising strategy for the treatment of ischemia-reperfusion injury by combining natural active compounds with nanoparticles.

Ethics Declarations

All animal experimental protocols in this study were approved by the Animal Use and Care Committee of Wenzhou Medical University (Approval No. xmsq2021-0809) and were conducted in accordance with the Laboratory Animal Environment and Facilities (GB 14925-2010) and the Animal Research: Reporting of In Vivo Experiments (ARRIVE) 2.0 guidelines.

Funding

This study was supported by the Natural Science Fund of Ningbo (2022J214, 2022J258).

Disclosure

The authors report no conflicts of interest in this work.

References

1. Hilkens NA, Casolla B, Leung TW, et al. Stroke. *Lancet*. 2024;403(10446):2820–2836. doi:10.1016/S0140-6736(24)00642-1
2. Abdelsalam SA, Renu K, Zahra HA, et al. Polyphenols mediate neuroprotection in cerebral ischemic stroke-an update. *Nutrients*. 2023;15(5):1107. doi:10.3390/nu15051107
3. Wang Y, Mulder IA, Westendorp WF, et al. Immunothrombosis in acute ischemic stroke. *Stroke*. 2025;56(2):553–563. doi:10.1161/STROKEAHA.124.048137
4. Emerich DF, Dean RL 3rd, Bartus RT. The role of leukocytes following cerebral ischemia: pathogenic variable or bystander reaction to emerging infarct? *Exp Neurol*. 2002;173(1):168–181. doi:10.1006/exnr.2001.7835
5. Pawluk H, Tafelska-Kaczmarek A, Sopońska M, et al. The influence of oxidative stress markers in patients with ischemic stroke. *Biomolecules*. 2024;14(9). doi:10.3390/biom14091130
6. Li XH, Yin FT, Zhou XH, et al. The signaling pathways and targets of natural compounds from traditional Chinese medicine in treating ischemic stroke. *Molecules*. 2022;27(10):3099.
7. He F, Zeng F, Situ X, et al. Detection and identification of imperatorin metabolites in rat, dog, monkey, and human liver microsomes by ultra-high-performance liquid chromatography combined with high-resolution mass spectrometry and compound discoverer software. *Biomed Chromatogr*. 2023;37(10):e5702. doi:10.1002/bmc.5702
8. Deng M, Xie L, Zhong L, et al. Imperatorin: a review of its pharmacology, toxicity and pharmacokinetics. *Eur J Pharmacol*. 2020;879:173124. doi:10.1016/j.ejphar.2020.173124
9. Ge JW, Deng S-J, Xue Z-W, et al. Imperatorin inhibits mitogen-activated protein kinase and nuclear factor kappa-B signaling pathways and alleviates neuroinflammation in ischemic stroke. *CNS Neurosci Ther*. 2022;28(1):116–125. doi:10.1111/cns.13748
10. Rodrigues VD, Detregiachi CRP, Dos Santos Bueno M, et al. Imperatorin: a furanocoumarin with potential in combating cancer development and progression-A comprehensive review. *Pharmaceuticals*. 2026;19(3):436. doi:10.3390/ph19030436
11. Veiga N, Diesendruck Y, Peer D. Targeted nanomedicine: lessons learned and future directions. *J Control Release*. 2023;355:446–457. doi:10.1016/j.jconrel.2023.02.010
12. Prakash S. Nano-based drug delivery system for therapeutics: a comprehensive review. *Biomed Phys Eng Express*. 2023;9(5):052002. doi:10.1088/2057-1976/acedb2
13. Gusić N, Ivković A, VaFaye J, et al. Nanobiotechnology and bone regeneration: a mini-review. *Int Orthop*. 2014;38(9):1877–1884. doi:10.1007/s00264-014-2412-0
14. Park H, Otte A, Park K. Evolution of drug delivery systems: from 1950 to 2020 and beyond. *J Control Release*. 2022;342:53–65. doi:10.1016/j.jconrel.2021.12.030
15. Dutt Y, Pandey RP, Dutt M, et al. Therapeutic applications of nanobiotechnology. *J Nanobiotechnology*. 2023;21(1):148. doi:10.1186/s12951-023-01909-z
16. Guo H, Zhao X, Duan Y, et al. Hollow mesoporous silica nanoparticles for drug formulation and delivery: opportunities for cancer therapy. *Colloids Surf B Biointerfaces*. 2025;249:114534. doi:10.1016/j.colsurfb.2025.114534
17. Abdollahi L, Dianat MJ, Marcos MD, et al. Hollow mesoporous silica nanoparticles: effective silica etching using tri-di- and mono-valent cations. *Biomater Adv*. 2022;133:112621. doi:10.1016/j.msec.2021.112621

18. Zhu C, Ma J, Ji Z, et al. Recent advances of cell membrane coated nanoparticles in treating cardiovascular disorders. *Molecules*. 2021;26(11):3428. doi:10.3390/molecules26113428
19. Feng L, Dou C, Xia Y, et al. Neutrophil-like cell-membrane-coated nanozyme therapy for ischemic brain damage and long-term neurological functional recovery. *ACS Nano*. 2021;15(2):2263–2280. doi:10.1021/acsnano.0c07973
20. Seligmann B, Chused TM, Gallin JI. Human neutrophil heterogeneity identified using flow microfluorometry to monitor membrane potential. *J Clin Invest*. 1981;68(5):1125–1131. doi:10.1172/JCI110356
21. Scieszka D, Lin Y-H, Li W, et al. NETome: a model to decode the human genome and proteome of neutrophil extracellular traps. *Sci Data*. 2022;9(1):702. doi:10.1038/s41597-022-01798-1
22. Tian X, Fan T, Zhao W, et al. Recent advances in the development of nanomedicines for the treatment of ischemic stroke. *Bioact Mater*. 2021;6(9):2854–2869. doi:10.1016/j.bioactmat.2021.01.023
23. Guo X, Liu G, Liu Y, et al. Nanomedicine-based therapeutic strategies for cerebral ischemia-reperfusion injury: from blood-brain barrier penetration to precision targeting. *Eur J Med Res*. 2026.
24. Yu Y, Fan M, Wu G, et al. Inflamed vessel–anchored release of H_2 across the blood-brain barrier for ischemic stroke neuroprotection. *Sci Adv*. 2026;12(9):eaea3355. doi:10.1126/sciadv.aea3355
25. Dong X, Gao J, Zhang CY, et al. Neutrophil membrane-derived nanovesicles alleviate inflammation to protect mouse brain injury from ischemic stroke. *ACS Nano*. 2019;13(2):1272–1283. doi:10.1021/acsnano.8b06572
26. Wan Y, Yu S-H. Polyelectrolyte controlled large-scale synthesis of hollow silica spheres with tunable sizes and wall thicknesses. *J Phys Chem C*. 2008;112(10):3641–3647. doi:10.1021/jp710990b
27. Walter K. What is acute ischemic stroke? *JAMA*. 2022;327(9):885. doi:10.1001/jama.2022.1420
28. Song D, Xu D, Zhang K, et al. Stroke mortality risk factors: global trends and regional variations (1990–2021). *J Am Heart Assoc*. 2025;14(12):e042107. doi:10.1161/JAHA.125.042107
29. Parvez S, Kaushik M, Ali M, et al. Dodging blood brain barrier with "nano" warriors: novel strategy against ischemic stroke. *Theranostics*. 2022;12(2):689–719. doi:10.7150/thno.64806
30. Babatunde KA, Wang X, Hopke A, et al. Chemotaxis and swarming in differentiated HL-60 neutrophil-like cells. *Sci Rep*. 2021;11(1):778. doi:10.1038/s41598-020-78854-6
31. Fang RH, Kroll AV, Gao W, et al. Cell membrane coating nanotechnology. *Adv Mater*. 2018;30(23):e1706759. doi:10.1002/adma.201706759
32. Mayadas TN, Cullere X, Lowell CA. The multifaceted functions of neutrophils. *Annu Rev Pathol*. 2014;9(1):181–218. doi:10.1146/annurev-pathol-020712-164023
33. Sun H, Hu L, Fan Z. β2 integrin activation and signal transduction in leukocyte recruitment. *Am J Physiol Cell Physiol*. 2021;321(2):C308–c316. doi:10.1152/ajpcell.00560.2020
34. Bouti P, Webbers SDS, Fagerholm SC, et al. β2 integrin signaling cascade in neutrophils: more than a single function. *Front Immunol*. 2020;11:619925. doi:10.3389/fimmu.2020.619925
35. Sekheri M, Othman A, Filep JG. β2 integrin regulation of neutrophil functional plasticity and fate in the resolution of inflammation. *Front Immunol*. 2021;12:660760. doi:10.3389/fimmu.2021.660760
36. Baden LR, El Sahly HM, Essink B, et al. Efficacy and safety of the mRNA-1273 SARS-CoV-2 vaccine. *N Engl J Med*. 2021;384(5):403–416. doi:10.1056/NEJMoa2035389
37. Keech C, Albert G, Cho I, et al. Phase 1-2 trial of a SARS-CoV-2 recombinant spike protein nanoparticle vaccine. *N Engl J Med*. 2020;383(24):2320–2332. doi:10.1056/NEJMoa2026920
38. Li Y, Li P, Wang W, et al. Nanoparticle-based drug delivery systems targeting inflammatory immune mechanisms in acute myocardial infarction: current advances and perspectives. *Front Cardiovasc Med*. 2025;12:1657300. doi:10.3389/fcvm.2025.1657300
39. Yuan L, Li Q, Bai D, et al. La(2)O(3) nanoparticles induce reproductive toxicity mediated by the Nrf-2/ARE signaling pathway in kunming mice. *Int J Nanomed*. 2020;15:3415–3431. doi:10.2147/IJN.S230949
40. Ye Y, Xie X, Bi Y, et al. Nrf2 alleviates acute ischemic stroke induced ferroptosis via regulating xCT/GPX4 pathway. *Free Radic Biol Med*. 2025;231:153–162. doi:10.1016/j.freeradbiomed.2025.02.040
41. Han JX, Wen C-X, Sun R, et al. The dorsal hippocampal CA3 regulates spatial reference memory through the CtBP2/GluR2 pathway. *FASEB J*. 2022;36(9):e22456. doi:10.1096/fj.202101609RR
42. Zhang J, Yao M, Jiang T, et al. A dorsal subiculum-medial mammillary body pathway for spatial memory. *Mol Psychiatry*. 2025;30(11):5045–5057. doi:10.1038/s41380-025-03087-w